ESO Phase 3 Data Release Description

Data Collection	XQ-100
Release Number	1
Data Provider	Sebastián López
Date	22.06.2016

Abstract

The Large Programme "Quasars and their absorption lines: a legacy survey of the high-redshift universe with VLT/XSHOOTER" (ID 189.A-0424, hereafter 'XQ-100') has produced a homogeneous and high-quality sample of echelle spectra of 100 QSOs at redshifts z ~ 3.5–4.5 observed with full spectral coverage from 315 to 2500 nm. XQ-100 is the largest spectroscopic survey to date of high-redshift QSOs with simultaneous rest-frame UV/optical coverage, and as such enables a wide range of extragalactic research, from cosmology and galaxy evolution to AGN astrophysics (López et al. 2016). This documents describes the first XQ-100 release, including all the reduced targets.

Overview of Observations

The observations were carried out in 'service mode' between 17.04.2012 and 23.02.2014. During this time XSHOOTER was mounted first on VLT unit 2 (until June 2013) and then on unit 3 (since November 2013). The targets were split up into two samples, brighter and fainter than magnitude R_{APM} = 18.0. The requested observing conditions were as follows:

- Seeing: 1.0″ (bright targets), 0.8″ (faint targets);
- Sky transparency: Clear;
- Airmass: $\delta > +20$: < 1.6; $+10 < \delta < 20$: < 1.5; $0 < \delta < +10$: < 1.4; $\delta < 0$: < 1.3;
- Lunar illumination: 50%;
- Moon distance: 45 degrees.

The airmass constraint was set according to each target's declination such that the target was observable above the set constraint for at least a 2 hours duration. Out of 100 targets, 88 were observed within specifications, and 12 "almost" within specifications (i.e., constraints were worse by 10%). 9 targets were observed twice and three targets were observed three times.
The following table summarizes the instrument observational setup:

Arm	Wavelength range [nm]	Slit width ″	Resolving power $\lambda/\Delta\lambda$	# of exposures		Integration time s	
				bright	faint	bright	faint
UVB	315–560	1.0	5100	2	4	890	880
VIS	540–1020	0.9	8800	2	4	840	830
NIR	1000–2480 (1800)	0.9	5300	2	4	900	900

The slit position was always set along the parallactic angle, except for five targets for which it was necessary to avoid contamination of a nearby bright object in the slit (these cases are relevant to a problem with the atmospheric dispersion corrector system, see below). Target acquisition was done in the R filter. The UVB and VIS were binned by a factor 2 in the dispersion direction. 53 targets with z > 4 were observed using a K-band blocking filter to avoid scattered light contamination in the J-band (Vernet et al. 2011); the upper limit of the NIR range in this case is put in parentheses. No blocking filter was used for the 47 targets with z < 4 targets, in order to include [OIII]λ5007 in the wavelength range.

Known issues

In March 2012 ESO reported that the atmospheric dispersion correctors (ADCs) started to fail occasionally. In August 2012 the ADCs were disabled for the rest of the observations. Based on large flux mismatches between arms and unexpected slopes in the quasar continuum, we determined the ADC issue had possibly affected 12 OBs (J1013+0650, J1126-0124, J1249-0159, J1352+1303, J1416+1811,

J1503+0419, J1524+2123, J1542+0955, J1552+1005, J1621-0042, J1723+2243, J2215-1611). Only 5 of these OBs (J1126-0124, J1249-0159, J1352+1303, J1503+0419, J2215-1611) were executed again at a later time.

In 6 cases (J0755+1345, J0113-2803, J1352+1303, J1401+0244, J1517+0511, J2239-0552), the OB execution was interrupted abruptly, leading to UVB and VIS frames with incomplete integration. Only 5 of these OBs (J0755+1345, J1352+1303, J1401+0244, J1517+0511, J2239-0552) were executed again at a later time.

Release Content

The full list of targets with all the relevant information is provided in the attached FITS frame `XQ-100_summary.fits`. The distribution of some key quantities is shown in Fig. 1, 2, and 3.
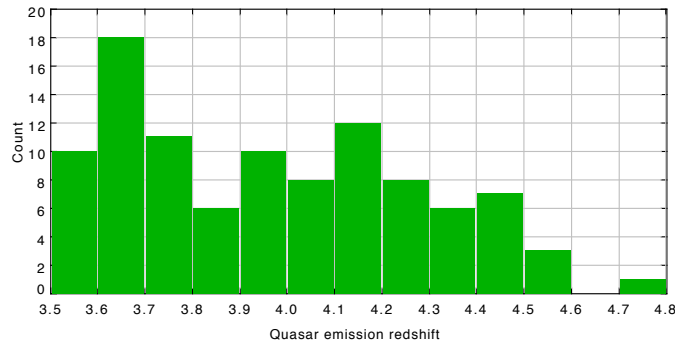

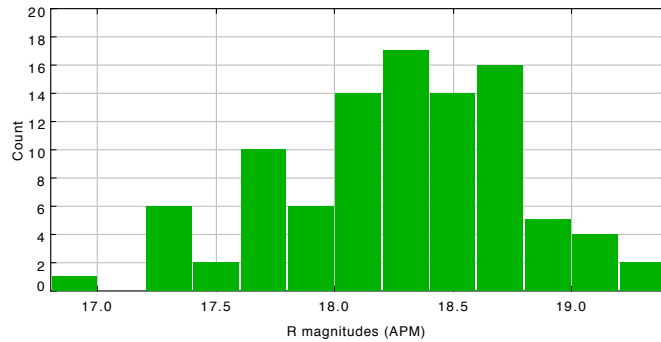**Fig. 1**. Distribution of the XQ-100 emission redshifts.

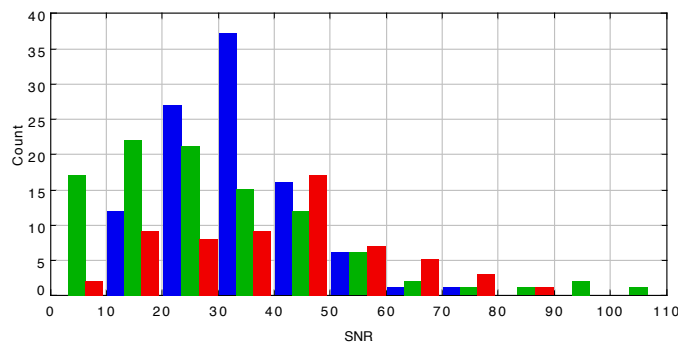**Fig. 2.** Distribution of the XQ-100 *R* magnitudes (APM).

Fig. 3. Distribution of SNR per pixel of the co-added spectra (see below) at three different rest-frame wavelengths: 170, 300, and 360 nm (blue, green, and red respectively). The SNR is computed in a window centered at those wavelengths and spanning ±1 nm.

Two types of data are provided for each target:

1. Individual UVB, VIS, and NIR spectra, with telluric correction and fitted QSO continuum;
2. A joint spectrum of the three arms together, rescaled to match the flux across arms.

For the targets observed without the K-band blocking filter, an additional file is provided for the NIR arm, containing the output of nodding reduction, whenever at least two exposures where available (see below). When a target was observed more than once at different epochs, we produced individual spectra of each execution of the OB. We discarded only the first executions when they were affected by the ADC issue, and the interrupted exposures (as their contribution was negligible due to the short integration time). We also produced a co-added spectrum putting together all epochs. QSO continua were determined in this case only on the co-added spectrum, while the telluric correction was performed only on individual epochs.

We define as "primary" spectra those with the best achievable SNR. For targets observed more than once, these are the co-added spectra. The following table summarizes the total number of spectra provided:

	UVB	VIS	NIR	NIR nodded	joint	
primary	100	100	100	47	100	
first execution	8	8	8	4	–	
second execution	8	8	8	5	–	
third execution	2	2	2	1	–	total
total	118	118	118	57	100	511

The following table gives the number of files included in the tarballs of single targets, depending on the K-band blocking filter (legend: e = number of exposures; a = number of co-added spectra; i = number of individual arm-by-arm spectra, including NIR nodded if applicable; c = number of joint spectra; t = total number of files):

K-band not blocked					K-band blocked				
e	a	i	c	t	e	a	i	c	t
(1	+ 0	) × 4	+ 1 =	5	(1	+ 0	) × 3	+ 1 =	4
(2	+ 1	) × 4	+ 1 =	13	(2	+ 1	) × 3	+ 1 =	10
(3	+ 1	) × 4	+ 1 =	17	(3	+ 1	) × 3	+ 1 =	13

Release Notes

Data treatment: overview

Data were reduced using an IDL pipeline developed by George D. Becker. We adopted custom tool instead of the standard ESO pipeline for two reasons: (i) obtain a better removal of the background and of the sky features, especially in the NIR arm, and (ii) perform an optimal extraction of the spectra, combining different exposures without a preliminar rectification of the spectral orders (see below). Tests on the ESO pipeline determined it was not adequate in both respects; for a more detailed discussion see López et al. (2016).

All targets were reduced with the same configuration of the reduction pipeline, in order to maintain the consistency across the sample. In addition to the standard reduction (including flux calibration and co-addition of different exposures), data were post-processed to remove the telluric features and fit the QSO continuum. Products of post-processing are an integral part of the current release.

Data reduction

The combined reduction strategy is based on the technique of Kelson (2003), wherein operations are performed on the un-rectified two-dimensional frames. This approach is recommended because the rectification of spectral orders necessarily entails a rebinning of the original pixel grid, which introduces spurious correlation across adjacent pixels. To apply the Kelson technique, we generated two-dimensional arrays of slit position and wavelength that served as the coordinate grid for sky modeling and one-dimensional spectrum extraction. A fiducial set of coordinate arrays for each arm was registered to individual science frames using the measured positions of sky and/or arc lines.
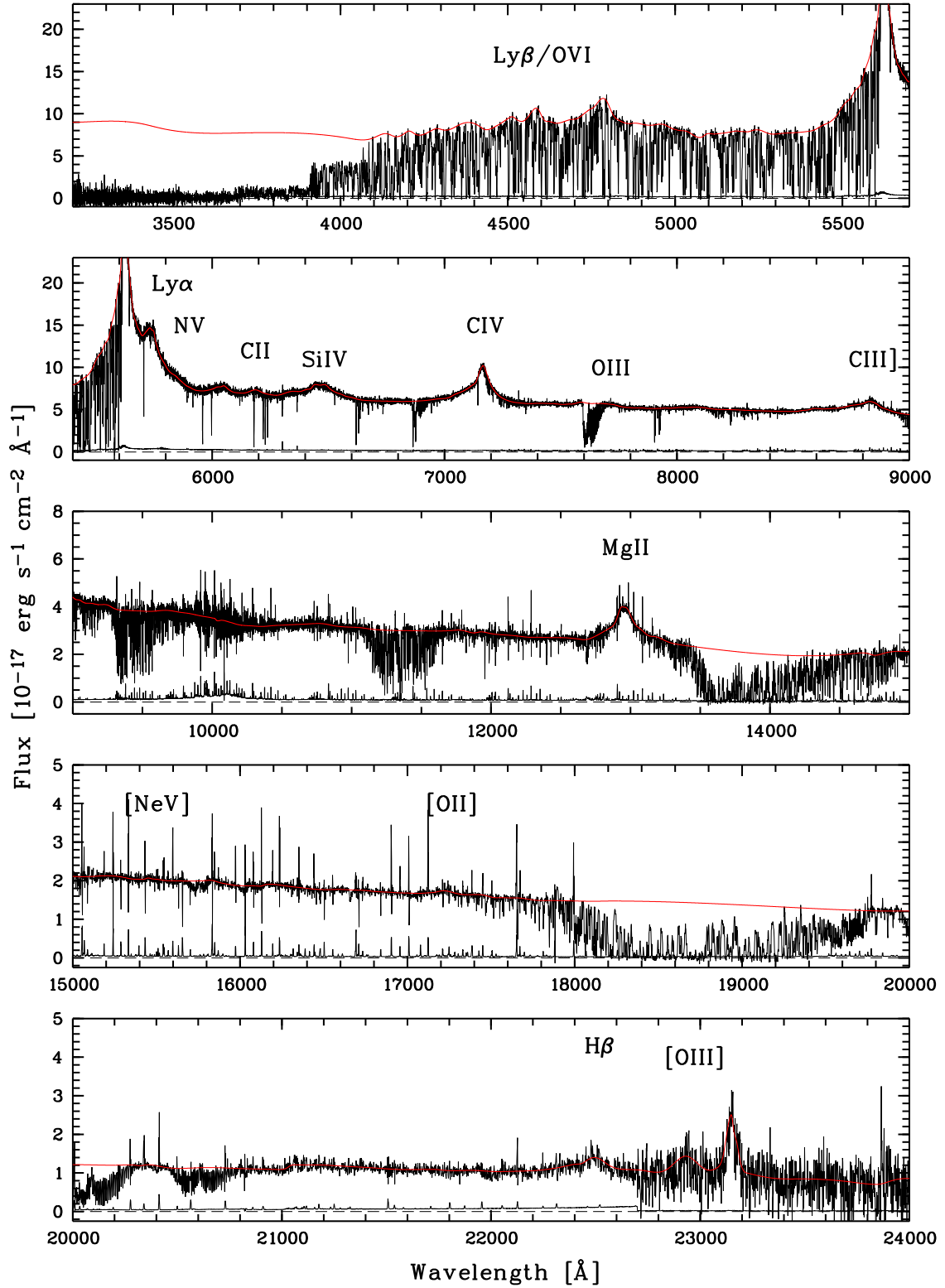
Fig. 4. XQ-100 spectrum of QSO J1117+1311 at z = 3.622, a representative case of the whole sample in terms of SNR. The flux is not corrected for telluric absorption or rebinned for display purposes. Some emission lines are marked. The red line depicts a manually-placed continuum made of cubic splines (see § 4.2 for details).

4

Individual frames were bias subtracted (or dark subtracted, in the case of the NIR arm) and flat-fielded. The sky emission in each order was then modeled using a B-spline and subtracted. To avoid adding significant extra noise in the NIR arm, composite dark frames were generated from multiple (~10) dark exposures with matching integration times. This approach was found to remove the fixed pattern noise in the NIR to the extent that the sky emission could generally be well modeled in each exposure independently, without subtracting a nodded frame, thus avoiding a factor of $\sqrt{2}$ penalty in the background noise. The exception to this was the reddest NIR order (2270-2480 nm), which is problematic because it is vignetted by a baffle designed to mask stray light (see `http://www.eso.org/observing/dfo/quality/XSHOOTER/qc/problems/problems_xshooter.html`). To obtain information for this order, NIR data of all targets observed without the K-band blocking filter were reduced also in nodding mode. The SNR of these spectra is significantly worse than that of their non-nodded counterparts; only the last order of nodded spectra (which is missing in the non-nodded ones) should be used for science.

Following sky subtraction, the counts in the two-dimensional frames were flux calibrated using response curves generated from observations of spectro-photometric standard stars. Standards observed close in time to the science observations were generally used. For a limited number of objects, however, the temporally-closest star was not optimal and unexpected features were observed in the flux-calibrated spectra. In these cases, a fiducial response curve was used to produce an additional flux-calibrated spectrum.

A single one-dimensional spectrum was then extracted simultaneously from across all orders and all exposures of a given object (in a single arm). A fixed velocity step was applied to the one-dimensional extracted spectra; this is the only rebinning involved in the reduction procedure. Velocity bins for the three arms were chosen to provide roughly 3 pixels per FWHM, taking the nominal XSHOOTER resolving power for the adopted slits: the values are 20 km s^{-1} for the UVB, 11 km s^{-1} for the VIS, and 19 km s^{-1} for the NIR. Wavelengths are calibrated to the vacuum-heliocentric system.

Science reduction was performed on different arms separately. We also produced joint spectra of the three arms together, by cutting and pasting the arms at fixed wavelengths (560 nm for the UVB-VIS interface; 1012.5 nm for the VIS-NIR interface). The last order of the NIR, when available, was also cut and pasted from the nodded spectra to the non-nodded ones (at 2270 nm). The maximum wavelength of the joint spectra was fixed at 1800 nm for the K-band blocked data and at 2500 nm otherwise. Median flux values in the superposition regions were used to equalize the VIS and NIR arms to the flux level of the UVB arm. The equalization was only meant to avoid occasional jumps across the arms (due to inaccuracies in flux calibration: see below); the flux values of the joint spectra should not be regarded as more reliable that those of the arm-by-arm spectra.

For each joint spectrum, a reduction quality parameter (saved in column `RED_QUAL` of the catalogue table, and separately also in columns `RED_QUAL_1`, `RED_QUAL_2`, and `RED_QUAL_3` for the different executions, when applicable; see below) has been computed as a sum of powers of two, according to the following code:

- 0 – OK.
- 1 – Flat frames and/or flux standard stars from a different night used for the reduction (not a quality issue; just for information).
- 2 – Spike residuals across orders in the UVB.
- 4 – Fluctuations in the VIS continuum.
- 8 – Interrupted execution (interrupted frames were not used for the reduction).
- 16 – Execution affected by the ADC issue (affected frames were not used when the execution had been repeated).

An example of reduced spectrum (with super-imposed continuum, see below) is given in Fig. 4.

Removal of telluric features

Telluric absorption affects spectra in both the VIS and NIR arms. Correcting these airmass-dependent spectral features using standard star spectra, even taken relatively close in time to the science targets, can become highly non-trivial due to the rapidly changing NIR atmospheric transparency. Instead, we opted to derive corrections using model transmission spectra based on the ESO SKYCALC Cerro Paranal Advanced Sky Model (Noll et al. 2012; Jones et al. 2013), version 1.3.5. The SKYCALC models are a function of both airmass and precipitable water vapor (PWV) and span a grid in these parameters providing a spectral resolution of R = 100 000. These corrections were applied to individual-epoch spectra of all XQ-100 sources.

Synthetic atmospheric transmission spectra based on the SKYCALC models were fit separately to each VIS and NIR one-dimensional spectrum as a means to remove the observed telluric absorption fetures. The skymodel airmass and PWV parameters, as well as a velocity offset and Gaussian FWHM smoothing kernel, were interactively adjusted for each spectrum in order to minimize the residuals in the mod-

el-subtracted spectrum over spectral regions observed to have moderate amounts of absorption. Following this initial, interactive parameter selection, an automated parameter selection was performed that searched a grid of only airmass and PWV values in a narrow grid, relative to the best-selected parameters from the interactive search. Multiple sets of "best-fit" automated parameters were determined for each spectrum by maximizing the SNR measured in the model-subtracted VIS or NIR spectrum over each of the wavelength regions listed above, separately, as well as an average SNR based on all VIS or NIR regions, respectively. The set of parameters used to create the final telluric-correction model was selected by eye from these multiple, best, model-subtracted spectra.

The telluric correction models were fit to all available spectra: this includes spectra of the individual executions of the OBs, as well as co-added spectra (note, however, that correction is less effective on the latter; this is a result of the spectra being co-added *before* telluric corrections).

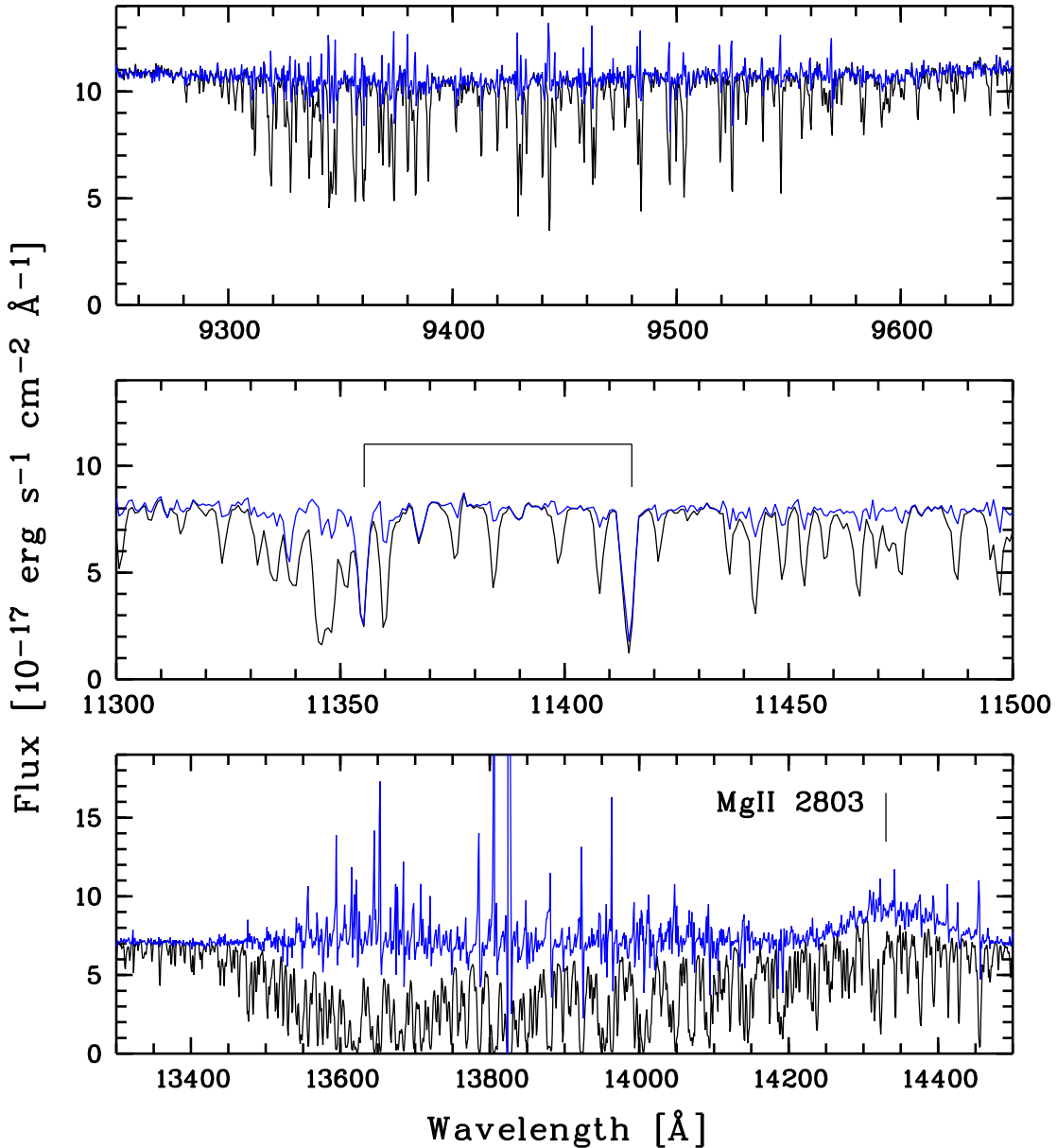An example of the results of telluric correction is given in Fig. 5.

Fig. 5. Spectrum of target J0003 2603 ($z = 4.125$) before (black) and after (blue) telluric corrections. Three spectral windows with strong telluric absorption are shown. In the middle panel the tickmarks above the spectrum indicate two FeII absorption lines, 258 and 260 nm, associated with the $z = 3.390$ DLA. In the bottom panel note how the MgII emission line stands out in the corrected spectrum.

Continuum fitting

The manually-placed continuum was completed by selecting points along the QSOs continuum free of absorption (by eye) as knots for a cubic spline fit. The code used for the continuum fitting is available at `https://github.com/trystynb/ContFit`.

The continuum placement was visually inspected and adjusted such that the final fit resides within the variations of regions with clean continuum. The accuracy of the fits is as good or better than the signal-to-noise of these clean continuum regions. As the continuum fits were created for accurate DLA metal line abundances (Berg et al; submitted), the fits around DLA metal lines have undergone multiple revisions compared to other regions of the spectra. The continuum placement in the Lyman-α forest is highly subjective due to the lack of clean QSO continuum (e.g. Kirkman et al. 2005), and is particularly difficult to identify around the Lyman-α absorption of DLAs. The continuum around a DLA's Lyman-α absorption features in the XQ-100 sightlines requires further refinement on a case-by-case basis to match the N(HI) fits of the Lyman-α wings (as implemented in Sanchez-Ramirez et al. 2016).

When the continuum is unknown, the spline knots were placed at a constant (high) flux at: (i) The Lyman limit if one or more obvious Lyman limits systems are clearly present, and (ii) Telluric features (near observed wavelengths 690, 760, 945, 1140, and 1400 nm). In some sightlines, there are strong absorption features ontop of the Lyman-α emission line of the QSO, such that continuum of the emission line is not well constrained (particularly near the peak of the emission). In cases with this strong absorption present, the continuum on the Lyman-α emission is assumed to follow the interpolation from the cubic spline fit to the surrounding continuum knots.

Known issues

In some cases the flux values in adjacent arms (especially VIS and NIR) do not match exactly and a gap is observed. A small mismatch is expected and depends on seeing conditions, since slit widths are different in each arm and the standard stars, used for flux calibration, are all taken with a 5″ slit. However, in a few spectra a larger mismatch is observed, which cannot be attributed to slit losses only.

We investigate the most severe cases of mismatch (> 30% across arms, affecting 12 out of 100 targets) and were able to explain it as a co-addition of three causes:

1. the ADC issue;
2. a sudden interruption in the OB execution, which produced UVB and VIS frames with shorter integration time (when this happens, NIR frames are automatically discarded); these frames were initially taken into account in the co-addition procedure;
3. problems with flat-fielding.

In 6 out 12 cases (J0113-2803, J1013+0650, J1524+2123, J1552+1005, J1621-0042, J1723+2243), the affected OB was not re-executed, and the mismatch could not be recovered. For the repeated OBs (J1352+1303, J1401+0244, J1517+0511) and for the bad flat-fielding cases (J0920+0725, J0937+0828, J0959+1312), attempts were made to alleviate the mismatch. Interrupted frames were discarded and different master flat frames were used, depending on situation. The first remedy proved to be successful for all the interested targets, and motivated the choice to generally discard the interrupted frames from co-added spectra (see above). The second remedy proved to be only marginally successful for the affected OBs. Since an *ad hoc* treatment of individual targets was beyond the scope of this release and would have compromised the consistency of the reduction process, we decided not to undertake any further action in this sense.

We remark flux calibration of XQ-100 spectra should *not* be taken as absolute. The spectral shape was correctly reconstructed and the flux values can be taken as order-of-magnitude estimates, but they must not be considered as reliable when accurate flux calibration is required. As a short-slit echelle spectrograph, XSHOOTER is in general sub-optimal for flux measurements. Better results can be achieved only through spectral templates obtained with long-slit instruments, or using the available photometry information for the targets; such alternative approaches might be adopted by a future XQ-100 release. The precision of flux calibration has been estimated from the standard deviation of the rescaling factors used to adjust the arms when creating the joint spectra; this value, expressed as a round percentage and included in the header of the data products, must be regarded as a lower limit.

Data Format

Files Types

All data products are formatted as FITS tables. The naming convention is:

- For the individual arm-by-arm spectra: `[target]_[exec]_[arm].fits`;
- For the joint spectra: `[target]_rescale.fits`;

where `[target]` is the target name in shortened J2000 coordinates (JNNNN+NNNN or JNNNN+NNNN), `_[exec]` is the optional execution suffix (`_1`, `_2`, `_3`, or nothing), and `[arm]` is the spectral arm, including the optional nodding suffix for the NIR (`uvb`, `vis`, `nir`, or `nir_nod`). NIR nodded spectra are released as ancillary to NIR spectra, as they have been extracted only for some targets and not for the whole sample (see above). The individual arm-by-arm spectrum without the `_[exec]` suffix is to be regarded as the primary spectrum for the given target in all cases.

The general list of table columns is `WAVE`, `FLUX`, `ERR_FLUX`, `CONTINUUM`, `FLUX_TELL_CORR`, `ERR_FLUX_TELL_CORR`: Some of these columns may be missing, though, as the continuum is computed only on arm-by-arm primary spectra, and the telluric correction is computed only on VIS, NIR, and NIR nodded spectra, separately for each executions. Depending on this constraints, the lists of columns are:

- UVB primary spectra: `WAVE`, `FLUX`, `ERR_FLUX`, `CONTINUUM`;
- UVB single-execution spectra: `WAVE`, `FLUX`, `ERR_FLUX`;
- Non-UVB primary spectra, when only one execution is available: `WAVE`, `FLUX`, `ERR_FLUX`, `CONTINUUM`, `FLUX_TELL_CORR`, `ERR_FLUX_TELL_CORR`;
- Non-UVB primary spectra, when multiple executions are available: `WAVE`, `FLUX`, `ERR_FLUX`, `CONTINUUM`;
- Non-UVB single-execution spectra: `WAVE`, `FLUX`, `ERR_FLUX`, `FLUX_TELL_CORR`, `ERR_FLUX_TELL_CORR`;
- Joint spectra: `WAVE`, `FLUX`, `ERR_FLUX`;

The column description is as follows:

- `WAVE`: wavelength in the vacuum-heliocentric system (nm);
- `FLUX`: flux density (erg cm^{-2} s^{-1} nm^{-1});
- `ERR_FLUX`: error on the flux density (erg cm^{-2} s^{-1} nm^{-1});
- `CONT_FLUX`: continuum flux (erg cm^{-2} s^{-1} nm^{-1});
- `TELL_CORR_FLUX`: same as `FLUX`, but with the telluric features removed (erg cm^{-2} s^{-1} nm^{-1});
- `ERR_TELL_CORR_FLUX`: error on `TELL_CORR_FLUX` (erg cm^{-2} s^{-1} nm^{-1}).

A catalogue table `XQ-100_summary.fits` is also available. The column description for this table is as follows (cells in columns labeled with `_1`, `_2`, `_3` are filled only when the corresponding target has been observed more than once):

1. `OBJECT`: target designation, as it appears in the header of the data products;
2. `RA_J2000`: target right ascension (deg, J2000.0);
3. `DEC_J2000`: target declination (deg, J2000.0);
4. `z_QSO`: quasar emission redshift, estimated by Principal Component Analysis;
5. `N_OBS`: number of observing epochs;
6. `MJD_OBS`: start of observations (d);
7. `MJD_OBS_1`: start of observations (1st execution only) (d);
8. `MJD_OBS_2`: start of observations (2nd execution only) (d);
9. `MJD_OBS_3`: start of observations (3rd execution only) (d);
10. `MJD_END`: end of observations (d);
11. `MJD_END_1`: end of observations (1st execution only) (d);
12. `MJD_END_2`: end of observations (2nd execution only) (d);
13. `MJD_END_2`: end of observations (3rd execution only) (d);
14. `SEEING_MIN`: minimum seeing from ESO.TEL.IA.FWHM keyword;
15. `SEEING_MIN_1`: minimum seeing from ESO.TEL.IA.FWHM keyword (1st execution only);
16. `SEEING_MIN_2`: minimum seeing from ESO.TEL.IA.FWHM keyword (2nd execution only);
17. `SEEING_MIN_3`: minimum seeing from ESO.TEL.IA.FWHM keyword (3rd execution only);
18. `SEEING_MAX`: maximum seeing measured at the start or at the end of integrations;
19. `SEEING_MAX_1`: maximum seeing from ESO.TEL.IA.FWHM keyword (1st execution only);
20. `SEEING_MAX_2`: maximum seeing from ESO.TEL.IA.FWHM keyword (2nd execution only);
21. `SEEING_MAX_3`: maximum seeing from ESO.TEL.IA.FWHM keyword (3rd execution only);
22. `SNR_170`: SNR in a 1 nm window around 170 nm (rest-frame);
23. `SNR_170_1`: SNR in a 1 nm window around 170 nm (1st execution only) (rest-frame);
24. `SNR_170_2`: SNR in a 1 nm window around 170 nm (2nd execution only) (rest-frame);
25. `SNR_170_3`: SNR in a 1 nm window around 170 nm (3rd execution only) (rest-frame);
26. `SNR_300`: SNR in a 1 nm window around 300 nm (rest-frame);

27. `SNR_300_1`: SNR in a 1 nm window around 300 nm (1st execution only) (rest-frame);
28. `SNR_300_2`: SNR in a 1 nm window around 300 nm (2nd execution only) (rest-frame);
29. `SNR_300_3`: SNR in a 1 nm window around 300 nm (3rd execution only) (rest-frame);
30. `SNR_360`: SNR in a 1 nm window around 360 nm (rest-frame);
31. `SNR_360_1`: SNR in a 1 nm window around 360 nm (1st execution only) (rest-frame);
32. `SNR_360_2`: SNR in a 1 nm window around 360 nm (2nd execution only) (rest-frame);
33. `SNR_360_3`: SNR in a 1 nm window around 360 nm (3rd execution only) (rest-frame);
34. `RED_QUAL`: reduction quality parameter (see above).
35. `RED_QUAL_1`: reduction quality parameter (1st execution only).
36. `RED_QUAL_2`: reduction quality parameter (2nd execution only).
37. `RED_QUAL_3`: reduction quality parameter (3rd execution only).
38. `HR_FLAG`: high-resolution spectrum flag;
39. `JOHNSON_MAG_B`: *B* magnitudes in Johnson system;
40. `JOHNSON_MAG_V`: *V* magnitudes in Johnson system;
41. `JOHNSON_MAG_R`: *R* magnitudes in Johnson system;
42. `SDSS_PSF_MAG_u`: SDSS PSF *u* magnitudes;
43. `SDSS_ERR_PSF_MAG_u`: Error on SDSS PSF *u* magnitudes;
44. `SDSS_PSF_MAG_g`: SDSS PSF *g* magnitudes;
45. `SDSS_ERR_PSF_MAG_g`: Error on SDSS PSF *g* magnitudes;
46. `SDSS_PSF_MAG_r`: SDSS PSF *r* magnitudes;
47. `SDSS_ERR_PSF_MAG_r`: Error on SDSS PSF *r* magnitudes;
48. `SDSS_PSF_MAG_i`: SDSS PSF *i* magnitudes;
49. `SDSS_ERR_PSF_MAG_i`: Error on SDSS PSF *i* magnitudes;
50. `SDSS_PSF_MAG_z`: SDSS PSF *z* magnitudes;
51. `SDSS_ERR_PSF_MAG_z`: Error on SDSS PSF *z* magnitudes;
52. `DR7Q_MATCH`: match in DR7Q spectroscopy;
53. `DR7Q_LATE`: DR7Q plate number;
54. `DR7Q_MJD`: DR7Q spectroscopic MJD (d);
55. `DR7Q_FIBER`: DR7Q fiber number (d);
56. `DR12Q_MATCH`: match in DR12Q spectroscopy;
57. `DR12Q_N`: number of spectroscopic observations in DR12Q;
58. `DR12Q_PLATE_1`: DR12Q plate number (1st observation);
59. `DR12Q_MJD_1`: DR12Q spectroscopic MJD (1st observation) (d);
60. `DR12Q_FIBER_1`: DR12Q fiber number (1st observation) (d);
61. `DR12Q_PLATE_2`: DR12Q plate number (2nd observation);
62. `DR12Q_MJD_2`: DR12Q spectroscopic MJD (2nd observation) (d);
63. `DR12Q_FIBER_2`: DR12Q fiber number (2nd observation) (d);
64. `FIRST_MATCH`: match in FIRST;
65. `FIRST_FLUX`: FIRST flux at 20 cm (mJy);
66. `FIRST_SNR`: SNR of FIRST detection;
67. `TMASS_MATCH`: matched in 2MASS;
68. `TMASS_MAG_J`: 2MASS *J* magnitudes;
69. `TMASS_ERR_MAG_J`: error on 2MASS *J* magnitudes;
70. `TMASS_SNR_J`: SNR of 2MASS detection in *J* bands;
71. `TMASS_MAG_H`: 2MASS *H* magnitudes;
72. `TMASS_ERR_MAG_H`: error on 2MASS *H* magnitudes;
73. `TMASS_SNR_H`: SNR of 2MASS detection in *H* bands;
74. `TMASS_MAG_K`: 2MASS *K* magnitudes;
75. `TMASS_ERR_MAG_K`: error on 2MASS *K* magnitudes;
76. `TMASS_SNR_K`: SNR of 2MASS detection in *K* bands;
77. `TMASS_RD_FLAG`: 2MASS rd flag;
78. `WISE_MATCH`: match in WISE;
79. `WISE_MAG_w1`: WISE *w1* magnitudes;
80. `WISE_ERR_MAG_w1`: error on WISE *w1* magnitudes;
81. `WISE_SNR_w1`: SNR of WISE detection in *w1* bands;
82. `WISE_RCHI2_w1`: WISE reduced chi-squared in *w1* bands;
83. `WISE_MAG_w2`: WISE *w2* magnitudes;
84. `WISE_ERR_MAG_w2`: error on WISE *w2* magnitudes;
85. `WISE_SNR_w2`: SNR of WISE detection in *w2* bands;
86. `WISE_RCHI2_w2`: WISE reduced chi-squared in *w2* bands;
87. `WISE_MAG_w3`: WISE *w3* magnitudes;
88. `WISE_ERR_MAG_w3`: error on WISE *w3* magnitudes;
89. `WISE_SNR_w3`: SNR of WISE detection in *w3* bands;

90. `WISE_RCHI2_w3`: WISE reduced chi-squared in *w3* bands;
91. `WISE_MAG_w4`: WISE *w4* magnitudes;
92. `WISE_ERR_MAG_w4`: error on WISE *w4* magnitudes;
93. `WISE_SNR_w4`: SNR of WISE detection in *w4* bands;
94. `WISE_RCHI2_w4`: WISE reduced chi-squared in *w4* bands;
95. `WISE_CC_FLAG`: WISE confusion and contamination flag;
96. `WISE_PH_QUAL`: WISE photometric quality flag;

Acknowledgements